NONLINEAR PROPERTIES OF STRUCTURAL HETEROGENEOUS PHOTONIC CRYSTAL FIBERS WITH As_2Se_3 SUBSTRATE

Nguyen Thi Thuy[a*], Dao Van Hung[b]

[a]University of Education, Hue University, Thua Thien Hue, Vietnam
[b]Naval Academy, Khanh Hoa, Vietnam
[*]Corresponding author: Email: ntthuy@hueuni.edu.vn

Article history
Received: October 4th, 2021
Received in revised form: November 3rd, 2021 | Accepted: November 8th, 2021
Available online: December 6th, 2021

Abstract

We examine the possibility of improving the nonlinear properties of photonic crystal fibers (PCFs) with As_2Se_3 substrates by creating a difference in the diameters of the air holes of the rings around the core. With the new design, all-normal dispersion properties, small effective mode area, high nonlinear coefficient, and low confinement loss were achieved in the long-wavelength range of 2.0–7.0 µm. The highest nonlinear coefficient is 4414.918 $W^{-1}.km^{-1}$ at 4.5 µm for the lattice constant (Λ) of 3.0 µm and the filling factor (d/Λ) of 0.85, while the lowest loss is 1.823×10^{-21} dB/cm with Λ = 3.5 µm and d/Λ = 0.8. Based on the numerical simulation results, the characteristics of two optimal structures have been analyzed in detail to guide the application in supercontinuum generation.

Keywords: All-normal dispersion; High nonlinear coefficient; Low confinement loss; Photonic crystal fibers with As_2Se_3 substrates.

DOI: http://dx.doi.org/10.37569/DalatUniversity.11.4.985(2021)

Article type: (peer-reviewed) Full-length research article

Copyright © 2021 The author(s).

Licensing: This article is licensed under a CC BY-NC 4.0

1. INTRODUCTION

In the past few decades, photonic crystal fibers (PCFs) (Knight, 2003) have been a topic of intense interest by scientists because of their ability to control the propagation of light. The high refractive index contrast between the core and cladding is strictly maintained to confine light in the core, which is the main mechanism for nonlinear effects. Silica PCFs are popular subjects of research because they exhibit numerous applications, such as optical communication (Kabir et al., 2020; Mohammadzadehasl & Noori, 2019), nonlinear optics (Park et al., 2020; Biswas et al., 2019), high power technology (Qi et al., 2018; Hasan et al., 2021), spectroscopy (Markin et al., 2017; Paul et al., 2020), and sensing applications such as gas sensing (Paul et al., 2018; Kaur & Singh, 2019) and chemical sensing (Podder et al., 2019; Eid et al., 2021) with its unique properties. Among them, supercontinuum (SC) generation (Lanh et al., 2019, 2020) has been widely studied, and outstanding results have been achieved in silica fiber. However, the operating wavelength range is limited because of the high matter loss above the 2-μm wavelength, so it is difficult to generate SC in the infrared region. Recently, non-silica compound glasses, such as chalcogenide, have shown many advantages in investigating nonlinear optical effects in PCFs because their large nonlinear refractive index compared to other glasses opens up the possibility of achieving interesting nonlinear properties at longer wavelengths. As_2Se_3, in the chalcogenide group, is an interesting substrate material for PCF; its nonlinear refractive index n_2 is equal to 2.4×10^{-17} m^2W^{-1} at 1.55 μm and is estimated to be about three orders of magnitude greater than that of pure silica. In 2015, Saini et al. (2015) presented a new design consisting of a triangular-core PCF in As_2Se_3-based chalcogenide glass with all-normal, nearly zero flat-top dispersion, with which ultra-broadband SC spanning 1.9–10 μm can be obtained. Zhao et al. (2017) proposed an As_2Se_3-based photonic quasi-crystal fiber with high nonlinearity and birefringence. A dispersion-engineered As_2Se_3 chalcogenide hexagonal PCF that can produce a mid-infrared SC spectral evolution from 2 μm to beyond 15 μm with a low peak power of 3 kW was numerically designed by Karim et al. (2018). Then in 2020, Gao et al. (2020) analyzed the characteristics of vector beams in mid-infrared waveband in an As_2Se_3 PCF with a small central hollow core, including the mode fields, confinement loss, effective refractive index, and chromatic dispersion. Also in 2020, numerical modeling of a PCF composed of a multicomponent chalcogenide glass system was reported by Chauhan et al. (2020) for highly coherent SC generation in the mid-infrared spectral region. In 2021, Bishwas et al. (2021) numerically demonstrated ultra-wideband mid-infrared SC generation in As_2Se_3-based square PCF with first inner ring air holes filled with liquid C_2H_5OH. It can be seen that the structure of PCF based on As_2Se_3 substrate has been widely studied because the change of structural parameters and the geometrical shape strongly influence the nonlinear characteristics of PCF.

In this paper, we present for the first time a novel structural design of PCF with an As_2Se_3 substrate. The difference in the diameter of the air holes in the second ring from the other rings leads to an improvement in the nonlinear properties of the fiber. We analyze in detail the nonlinear characteristics of the fiber on the basis of numerical simulation results and propose two optimal structures for SC applications.

2. NUMERICAL MODELING OF PCF PROPERTIES

The fundamental propagating mode in the core to generate nonlinear characteristics in the infrared wavelength region is simulated through a modified hexagonal-shaped PCF with an As_2Se_3 substrate. The air holes are positioned in a hexagonal array of diameter *d*, with the distance between the centers of the air holes given by the lattice constant (Λ). The filling factor (d/Λ) of the rings in the photonic cladding is designed to investigate the variation in the nonlinear quantities. Previous work (Saitoh et al., 2003) shows that the characteristics of PCFs can be effectively controlled by creating heterogeneity in the size of the air holes in the rings of the coating. The first ring near the core is mainly responsible for optimizing the flatness and the all-normal or anomalous properties of the dispersion, even the shift of the zero-dispersion wavelength (ZDW), while the second ring and the other rings govern the mode confinement loss, especially for higher modes. Therefore, we designed the air hole diameter of the second ring as $d_2 = 1.15d$, where *d* is the air hole diameter of the first and other rings, the filling factor d/Λ varies from 0.3 to 0.85 with a step of 0.05, and the values of Λ are 3.0 µm, and 3.5 µm. With such a design we obtained 24 structures, small PCF cores help the electromagnetic modes propagate over a wide range of wavelengths. The core diameter is defined by the formula $D_{core} = 2\Lambda - d$. The flexibility in controlling structural parameters to obtain minimal confinement loss and optimal dispersion is new in this design. The cross-section of the PCFs and the strongly confined light in the core are indicated in Figures 1a and 1b. The nonlinear optical parameters of the PCF, including effective index, chromatic dispersion, effective mode area, and confinement loss for different values of the lattice constant and the filling factor, are simulated in the 2–7 µm wavelength region with a perfectly matched layer as the boundary condition. The simulations use the finite element method and the commercial software, Lumerical Mode Solution multiphysics.

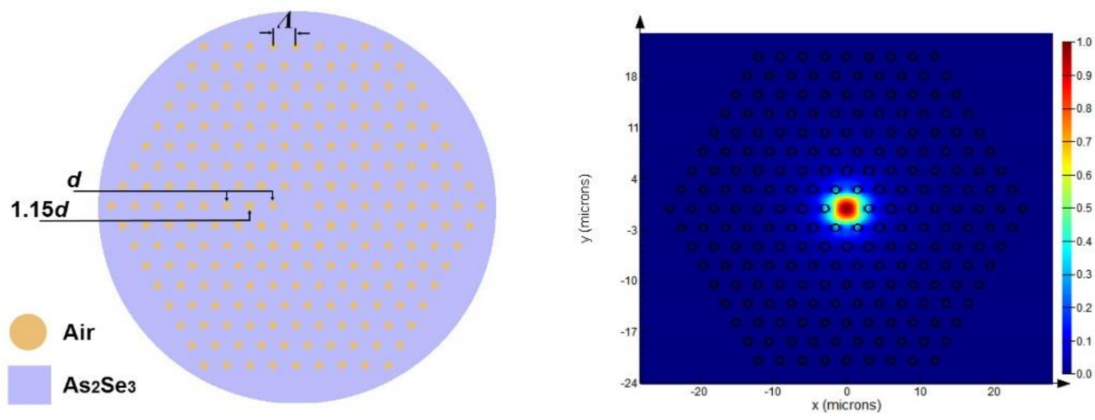

(a) (b)

Figure 1. The cross-section of PCFs (a) and the strongly confined light in the core (b)

3. SIMULATION RESULTS AND ANALYSIS

3.1. Effective refraction index

The refractive index of As_2Se_3 depends on the wavelength (λ in µm) and is calculated according to the Sellmeier equation (Ung & Skorobogatiy, 2010):

$$n^2 - 1 = \frac{2.234921^2 \lambda^2}{\lambda^2 - 0.24164^2} + \frac{0.347441^2 \lambda^2}{\lambda^2 - 19^2} + \frac{1.308575^2 \lambda^2}{\lambda^2 - 4 \times 0.24164^2}. \quad (1)$$

The real part of the effective refraction index as a function of wavelength for various *d/Λ* is presented in Figure 2. An increase in wavelength reduces the effective index of the fibers. The variation of the lattice constant *Λ* and the filling factor *d/Λ* also significantly changes the value of the effective refraction index. This value decreases with an increase in *d/Λ*, and the curves separate more clearly in the long-wavelength region (above 3.5 µm). This separation is more evident with *Λ* = 3.0 µm (Figure 2a). The refractive index of the medium varies when an intense input pulse propagates through the nonlinear medium, which causes the effective refraction index to change as well. The interaction ability of light in the nonlinear medium of small core PCFs is stronger than in large core PCFs, so the real part of the effective refraction index is larger in the case of *Λ* = 3.5 µm (Figure 2b).

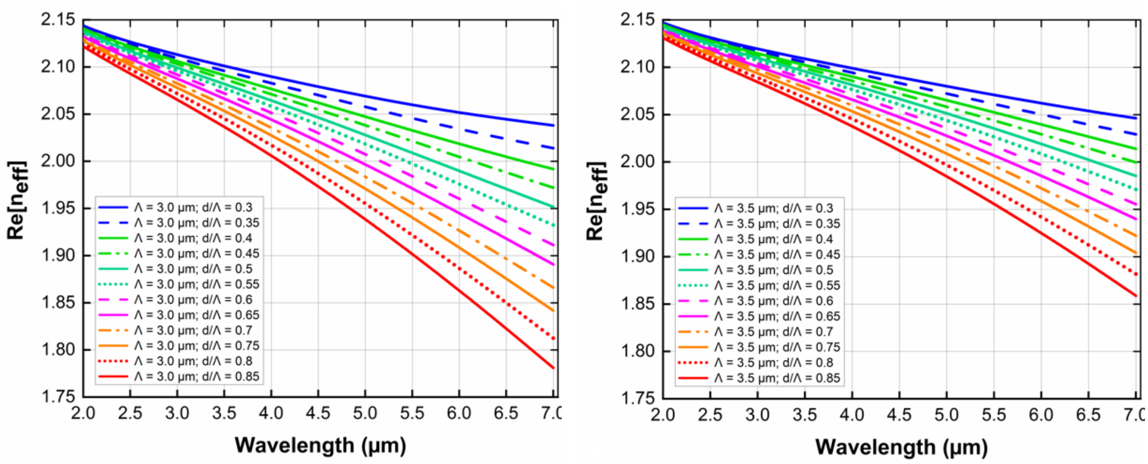

(a) (b)

Figure 2. The real part of the effective refraction index as a function of wavelength of PCFs with various *d/Λ* for (a) *Λ* = 3.0 µm, (b) *Λ* = 3.5 µm

The values of the real part of the effective refraction index for fibers with various *d/Λ* and *Λ* are calculated at 4.5 µm wavelength, which matches the expected pump wavelength to generate SC. The values are displayed in Tables 1a and 1b. For the case of *Λ* = 3.5 µm and *d/Λ* = 0.3, the refractive index reaches a maximum of 2.089. When *Λ* = 3.0 µm and *d/Λ* = 0.3, this value is 2.079, a slight decrease because of the small core. The small difference between the refractive indices for the two cases is 0.01.

Table 1a. Real part of the effective refraction index of PCFs with various *d/Λ* and *Λ* = 3.0 μm at 4.5 μm wavelength

λ (μm)	$Re[n_{\mathrm{eff}}]$					
	Λ = 3.0 μm, d/Λ = 0.3	Λ = 3.0 μm, d/Λ = 0.35	Λ = 3.0 μm, d/Λ = 0.4	Λ = 3.0 μm, d/Λ = 0.45	Λ = 3.0 μm, d/Λ = 0.5	Λ = 3.0 μm, d/Λ = 0.55
4.5	2.079	2.070	2.062	2.055	2.046	2.039
	Λ = 3.0 μm, d/Λ = 0.6	Λ = 3.0 μm, d/Λ = 0.65	Λ = 3.0 μm, d/Λ = 0.7	Λ = 3.0 μm, d/Λ = 0.75	Λ = 3.0 μm, d/Λ = 0.8	Λ = 3.0 μm, d/Λ = 0.85
4.5	2.030	2.021	2.010	2.000	1.987	1.973

Table 1b. Real part of the effective refraction index of PCFs with various *d/Λ* and *Λ* = 3.5 μm at 4.5 μm wavelength

λ (μm)	$Re[n_{\mathrm{eff}}]$					
	Λ = 3.5 μm, d/Λ = 0.3	Λ = 3.5 μm, d/Λ = 0.35	Λ = 3.5 μm, d/Λ = 0.4	Λ = 3.5 μm, d/Λ = 0.45	Λ = 3.5 μm, d/Λ = 0.5	Λ = 3.5 μm, d/Λ = 0.55
4.5	2.089	2.083	2.078	2.072	2.067	2.061
	Λ = 3.5 μm, d/Λ = 0.6	Λ = 3.5 μm, d/Λ = 0.65	Λ = 3.5 μm, d/Λ = 0.7	Λ = 3.5 μm, d/Λ = 0.75	Λ = 3.5 μm, d/Λ = 0.8	Λ = 3.5 μm, d/Λ = 0.85
4.5	2.054	2.047	2.040	2.032	2.022	2.012

3.2. Chromatic dispersion

Dispersion, i.e., the broadening of a pulse in propagation through optical fibers, is a very important factor for SC generation since it governs the SC spectrum expansion efficiency. In our simulations, the numerical calculations are repeated many times for each wavelength, and we try to divide points as much as possible in the survey wavelength range, so that chromatic dispersion *D* can be calculated accurately from the real part of the effective refraction index and the wavelength of the fundamental mode (Buczyński, 2004):

$$D = -\frac{\lambda}{c}\frac{d^2\left(\mathrm{Re}\left[n_{\mathrm{eff}}\right]\right)}{d\lambda^2} \tag{2}$$

where *c* is the speed of light.

The variation in chromatic dispersion with *Λ* and *d/Λ* is shown in Figure 3. The variation of the dispersion curves is quite large; they can intersect the zero-dispersion line at one or two points, which means that PCFs exhibit anomalous dispersion properties, including one or two ZDWs, in the investigated wavelength range. Interestingly, all-normal dispersions (negative dispersion), which are very significant in

SC spectrum expansion efficiency, have been achieved through a self-phase modulation and optical wave-breaking mechanism. Thus, the designed fibers exhibit both all-normal and anomalous dispersion with a shift of the ZDW toward longer wavelengths. With an increase of the filling factor *d/Λ*, there is a very rapid transition from all-normal to anomalous dispersion, and the dispersion curve becomes flatter and smoother. With the smaller core (*Λ* = 3.0 µm), we obtain two structures with all-normal dispersion when *d/Λ* = 0.3 and 0.35. Anomalous dispersions with two ZDWs were obtained for *d/Λ* ≤ 0.6; when *d/Λ* is greater than 0.6, anomalous dispersions with one ZDW prevail.

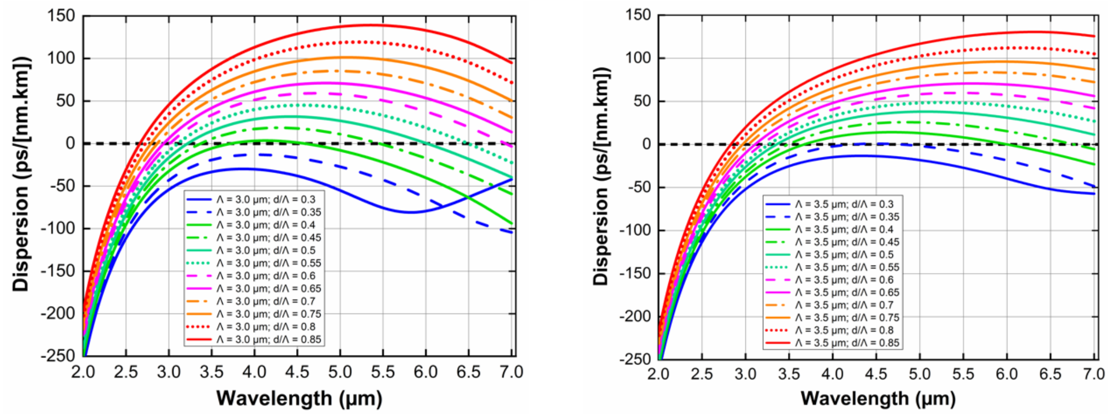

(a) (b)

Figure 3. Chromatic dispersion of PCFs with various *d/Λ* for (a) *Λ* = 3.0 µm, (b) *Λ* = 3.5 µm

The core diameter D_{core} has a substantial effect on the change of dispersion profile. Specifically, when *Λ* equals 3.5 µm (with the larger core), all-normal dispersion only exists with *d/Λ* = 0.3 (Figure 3b). From this, it can be predicted that when *Λ* exceeds 3.5 µm, all dispersion curves corresponding to the variation of *d/Λ* are in the anomalous state, i.e., no all-normal dispersion is observed in the wavelength region of interest. Figure 3b also shows the anomalous dispersions with two ZDWs that appear when *d/Λ* ≤ 0.45. For larger values of *d/Λ*, the dispersion is anomalous with one ZDW. Therefore, we can conclude that dispersion features can be controlled more effectively in smaller core PCFs because of their strong light confinement ability. At 4.5 µm wavelength, the dispersion values decrease slightly for *Λ* = 3.5 µm, as shown in Tables 2a and 2b. The dispersion curve is also flatter, which is very beneficial for SC generation in the infrared region. The smallest dispersion obtained is 0.90 ps.(nm.km)$^{-1}$ (*Λ* = 3.5 µm; *d/Λ* = 0.35) and the highest dispersion is 129.05 ps.(nm.km)$^{-1}$ (*Λ* = 3.0 µm; *d/Λ* = 0.85). The ZDW is important in the selection of the pump wavelength used for SC generation, which is calculated according to the variation of *d/Λ* and *Λ* of the PCFs. These values are given in Table 3. There are no ZDW values when *Λ* = 3.0 µm and *d/Λ* = 0.3 or 0.35, or when *Λ* = 3.5 µm and *d/Λ* = 0.3, because the dispersion curve does not cross the zero-dispersion line. On the other hand, one or two ZDW values can be found corresponding to anomalous dispersion properties as *d/Λ* increases because the number of ZDWs depends on the change of *Λ* and *d/Λ*. It can be seen that the variation in the filling factors of the second ring in the cladding has created a range of dispersion properties in the PCFs. Obviously, the dispersion characteristics are controllable by varying the air hole diameter of the rings in the cladding as well as by varying the filling factors and lattice constants. We obtained three PCFs with all-normal dispersion in the investigated wavelength range that were not found in previous studies (Cherif et al., 2010; Hui et al., 2018; Li et al., 2018; Karim et al., 2018; Wang et al., 2012). The all-normal dispersion property is an important factor for SC generation with large bandwidth.

Table 2a. Chromatic dispersion of PCFs with various *d/Λ* and *Λ* = 3.0 μm at 4.5 μm wavelength

λ (μm)	D (ps.(nm.km)$^{-1}$)					
	Λ = 3.0 μm, d/Λ = 0.3	Λ = 3.0 μm, d/Λ = 0.35	Λ = 3.0 μm, d/Λ = 0.4	Λ = 3.0 μm, d/Λ = 0.45	Λ = 3.0 μm, d/Λ = 0.5	Λ = 3.0 μm, d/Λ = 0.55
4.5	-37.97	-16.88	1.20	17.89	31.66	45.10
	Λ = 3.0 μm, d/Λ = 0.6	Λ = 3.0 μm, d/Λ = 0.65	Λ = 3.0 μm, d/Λ = 0.7	Λ = 3.0 μm, d/Λ = 0.75	Λ = 3.0 μm, d/Λ = 0.8	Λ = 3.0 μm, d/Λ = 0.85
4.5	58.54	69.64	82.60	96.83	112.42	129.05

Table 2b. Chromatic dispersion of PCFs with various *d/Λ* and *Λ* = 3.5 μm at 4.5 μm wavelength

λ (μm)	D (ps.(nm.km)$^{-1}$)					
	Λ = 3.5 μm, d/Λ = 0.3	Λ = 3.5 μm, d/Λ = 0.35	Λ = 3.5 μm, d/Λ = 0.4	Λ = 3.5 μm, d/Λ = 0.45	Λ = 3.5 μm, d/Λ = 0.5	Λ = 3.5 μm, d/Λ = 0.55
4.5	-13.63	0.90	13.82	24.52	34.98	43.52
	Λ = 3.5 μm, d/Λ = 0.6	Λ = 3.5 μm, d/Λ = 0.65	Λ = 3.5 μm, d/Λ = 0.7	Λ = 3.5 μm, d/Λ = 0.75	Λ = 3.5 μm, d/Λ = 0.8	Λ = 3.5 μm, d/Λ = 0.85
4.5	52.28	60.79	70.62	80.07	91.79	104.49

Table 3. Zero-dispersion wavelength of PCFs with various *d/Λ* and *Λ*

ZDW (μm)	Λ = 3.0 μm	Λ = 3.5 μm	ZDW (μm)	Λ = 3.0 μm	Λ = 3.5 μm
d/Λ = 0.3	-	-	d/Λ = 0.6	3.009 and 6.929	3.183
d/Λ = 0.35	-	4.219 and 4.778	d/Λ = 0.65	2.939	3.108
d/Λ = 0.4	3.722 and 4.593	3.670 and 6.004	d/Λ = 0.7	2.863	3.032
d/Λ = 0.45	3.368 and 5.460	3.485 and 6.769	d/Λ = 0.75	2.790	2.966
d/Λ = 0.5	3.218 and 6.017	3.354	d/Λ = 0.8	2.724	2.895
d/Λ = 0.55	3.102 and 6.499	3.266	d/Λ = 0.85	2.662	2.830

3.3. Effective nonlinearity

If the SC spectrum needs to be extended further, the nonlinear coefficient (γ) should be made as high as possible. The value of γ can be enhanced by using a material with a high nonlinear refractive index such as As_2Se_3, by designing a PCF with a smaller effective mode area (A_{eff}), or by a combination of both. The nonlinear coefficient of PCF is inversely proportional to the effective mode area, depending on the designed structural parameters, and is determined by the following formula (Saini et al., 2015):

$$\gamma(\lambda) = 2\pi \frac{n_2}{\lambda A_{eff}} \tag{3}$$

where n_2 is the nonlinear index of As_2Se_3, $\left(n_2 = 2.4\times10^{-17}\ \text{m}^2.\text{W}^{-1}\right)$ (Ung & Skorobogatiy, 2010), and A_{eff} is the characteristic nonlinearity of PCF, defined as in the following equation (Saini et al., 2015):

$$A_{eff} = \frac{\left(\int_{-\infty}^{\infty}\int_{-\infty}^{\infty} |E|^2\, dxdy\right)^2}{\int_{-\infty}^{\infty}\int_{-\infty}^{\infty} |E|^4\, dxdy} \tag{4}$$

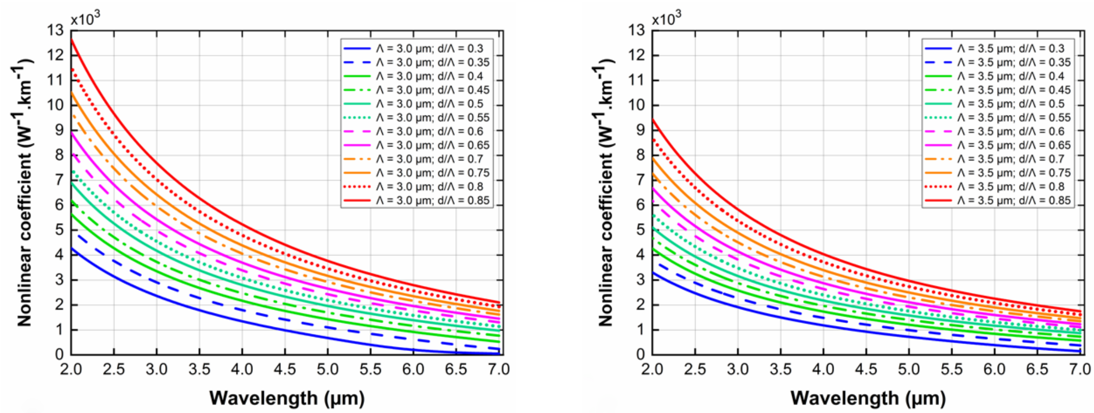

(a) (b)

Figure 4. The nonlinear coefficient as a function of wavelength for PCFs with various *d/Λ* and (a) *Λ* = 3.0 µm, (b) *Λ* = 3.5 µm

By using a highly nonlinear substrate material and designing a small core, we obtained PCFs with a high nonlinear coefficient. The effects of variation in wavelength, *d/Λ*, and *Λ* on the nonlinear coefficient are shown in Figure 4. The nonlinear coefficient has a large value in the short wavelength region and decreases with increasing wavelength. However, lattice parameters such as *d/Λ* and *Λ* make the nonlinear coefficient significantly different. The larger the core diameter, the smaller the effective mode area. So, with the larger core, the nonlinear coefficient drops in the studied wavelength region. The values of γ for Λ = 3.5 µm are smaller than for Λ = 3.0 µm (Figures 4a and 4b). In addition, as the filling factor increases, the nonlinear coefficient also increases very quickly. Tables 4a and 4b give the nonlinear coefficient of PCF for various d/Λ and Λ at 4.5 µm wavelength. The maximum and minimum values of γ are 4414.918 $W^{-1}.km^{-1}$ and 931.194 $W^{-1}.km^{-1}$, corresponding to Λ = 0.3 µm for d/Λ = 0.85 and Λ = 3.5 µm for d/Λ = 0.3, respectively.

Table 4a. The nonlinear coefficient of PCF for various *d/Λ* and *Λ* = 3.0 µm at 4.5 µm wavelength

λ (µm)	γ ($W^{-1}.km^{-1}$)					
	Λ = 3.0 µm, d/Λ = 0.3	Λ = 3.0 µm, d/Λ = 0.35	Λ = 3.0 µm, d/Λ = 0.4	Λ = 3.0 µm, d/Λ = 0.45	Λ = 3.0 µm, d/Λ = 0.5	Λ = 3.0 µm, d/Λ = 0.55
4.5	986.984	1414.709	1762.759	2046.027	2337.508	2590.456
	Λ = 3.0 µm, d/Λ = 0.6	Λ = 3.0 µm, d/Λ = 0.65	Λ = 3.0 µm, d/Λ = 0.7	Λ = 3.0 µm, d/Λ = 0.75	Λ = 3.0 µm, d/Λ = 0.8	Λ = 3.0 µm, d/Λ = 0.85
4.5	2857.662	3119.86	3426.585	3709.628	4048.43	4414.918

Table 4b. The nonlinear coefficient of PCF for various *d/Λ* and *Λ* = 3.5 µm at 4.5 µm wavelength

λ (µm)	γ ($W^{-1}.km^{-1}$)					
	Λ = 3.5 µm, d/Λ = 0.3	Λ = 3.5 µm, d/Λ = 0.35	Λ = 3.5 µm, d/Λ = 0.4	Λ = 3.5 µm, d/Λ = 0.45	Λ = 3.5 µm, d/Λ = 0.5	Λ = 3.5 µm, d/Λ = 0.55
4.5	931.194	1213.592	1445.361	1656.676	1848.808	2043.309
	Λ = 3.5 µm, d/Λ = 0.6	Λ = 3.5 µm, d/Λ = 0.65	Λ = 3.5 µm, d/Λ = 0.7	Λ = 3.5 µm, d/Λ = 0.75	Λ = 3.5 µm, d/Λ = 0.8	Λ = 3.5 µm, d/Λ = 0.85
4.5	2248.592	2448.706	2670.708	2898.187	3173.751	3439.961

3.4. Confinement loss

The confinement loss in the PCFs decreases very quickly under the influence of the filling factor d/Λ. The small confinement loss is the outstanding feature of our design. Figures 5a and 5b show the dependence of the confinement loss on wavelength with various d/Λ and Λ. When d/Λ is higher than 0.4, the confinement loss curves are almost coincident and asymptotically close to the horizontal axis. The lowest value that can be found is 1.823×10^{-21} dB/cm when Λ = 3.5 µm and d/Λ = 0.8 at 4.5 µm wavelength (Tables 5a and 5b). The confinement loss values of PCFs in our work are smaller than those of some previous publications (Li et al., 2018; Saini et al., 2015).

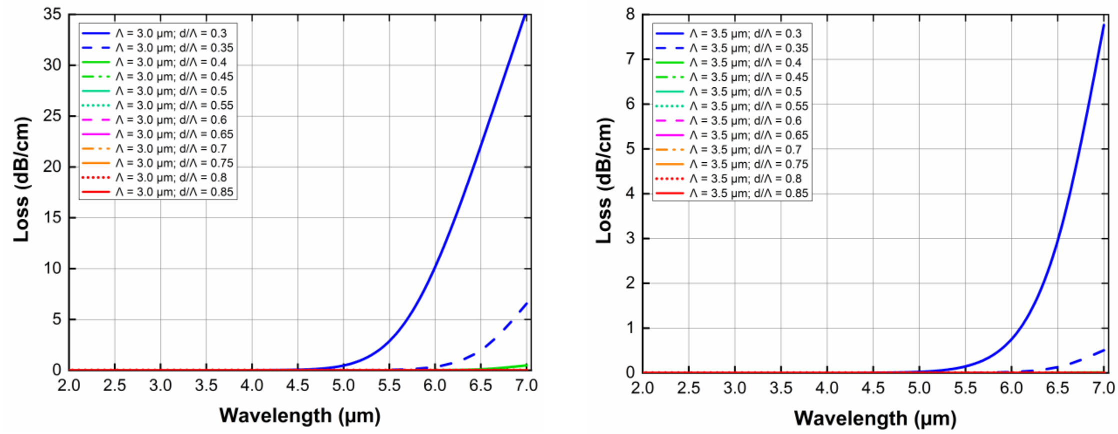

(a) (b)

Figure 5. The confinement loss as a function of wavelength for the fiber with various *d/Λ* and (a) *Λ* = 3.0 μm, (b) *Λ* = 3.5 μm

Table 5a. Confinement loss of PCFs with various *d/Λ* and *Λ* = 3.0 μm at 4.5 μm wavelength

λ (μm)	L_c (dB/cm)					
	Λ = 3.0 μm, d/Λ = 0.3	Λ = 3.0 μm, d/Λ = 0.35	Λ = 3.0 μm, d/Λ = 0.4	Λ = 3.0 μm, d/Λ = 0.45	Λ = 3.0 μm, d/Λ = 0.5	Λ = 3.0 μm, d/Λ = 0.55
4.5	5.042E-02	3.075E-04	3.011E-06	1.667E-08	6.595E-11	1.993E-13
	Λ = 3.0 μm, d/Λ = 0.6	Λ = 3.0 μm, d/Λ = 0.65	Λ = 3.0 μm, d/Λ = 0.7	Λ = 3.0 μm, d/Λ = 0.75	Λ = 3.0 μm, d/Λ = 0.8	Λ = 3.0 μm, d/Λ = 0.85
4.5	5.004E-16	6.497E-19	2.518E-21	5.468E-21	3.938E-21	5.83E-21

Table 5b. Confinement loss of PCFs with various *d/Λ* and *Λ* = 3.5 μm at 4.5 μm wavelength

λ (μm)	L_c (dB/cm)					
	Λ = 3.5 μm, d/Λ = 0.3	Λ = 3.5 μm, d/Λ = 0.35	Λ = 3.5 μm, d/Λ = 0.4	Λ = 3.5 μm, d/Λ = 0.45	Λ = 3.5 μm, d/Λ = 0.5	Λ = 3.5 μm, d/Λ = 0.55
4.5	2.98E-03	3.146E-05	2.349E-07	1.744E-09	1.107E-11	4.131E-14
	Λ = 3.5 μm, d/Λ = 0.6	Λ = 3.5 μm, d/Λ = 0.65	Λ = 3.5 μm, d/Λ = 0.7	Λ = 3.5 μm, d/Λ = 0.75	Λ = 3.5 μm, d/Λ = 0.8	Λ = 3.5 μm, d/Λ = 0.85
4.5	1.288E-17	1.317E-20	3.474E-21	1.906E-21	1.823E-21	2.552E-21

3.5. Optimization of the structural parameters of PCFs for SC generation

When the input pulse propagates in a nonlinear medium such as PCF, dispersion is the most important characteristic to be kept in mind, because it not only affects the widening, flatness, and high coherence of the spectrum, but it also governs the nonlinear effects, such as four-wave mixing, phase modulation, and the existence of solitons. In particular, SC generation with an all-normal dispersion PCF helps us create a single coherent, broadband flat-top pulse if the fiber is pumped at the wavelength (4.5 μm) with the flat dispersion closest to the wavelength of the maximum dispersion. For that reason, two PCFs that satisfy the above dispersion characteristics for SC generation were selected for analysis. Based on the simulation results, we propose two PCFs with Λ = 3.0 μm, d/Λ = 0.35 and Λ = 3.5 μm, d/Λ = 0.3, which have all-normal dispersions and are nearest to the zero-dispersion line. The structural parameters of the proposed PCFs, #F_1 and #F_2, are shown in Table 6.

Table 6. The structural parameters of the proposed PCFs

#	Λ (μm)	d/Λ	D_c (μm)
#F_1	3.0	0.35	4.95
#F_2	3.5	0.3	5.95

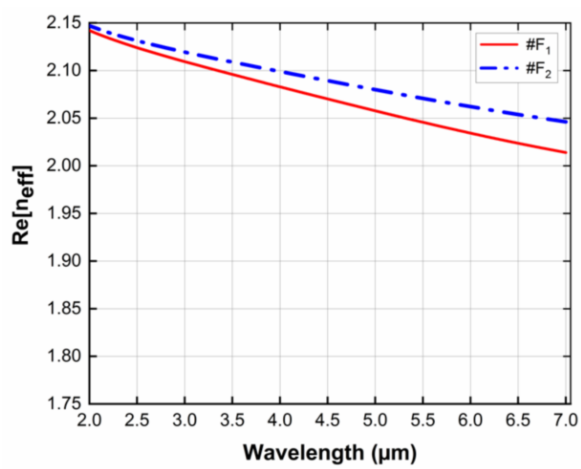

Figure 6. The real part of the effective refraction index of the proposed PCFs

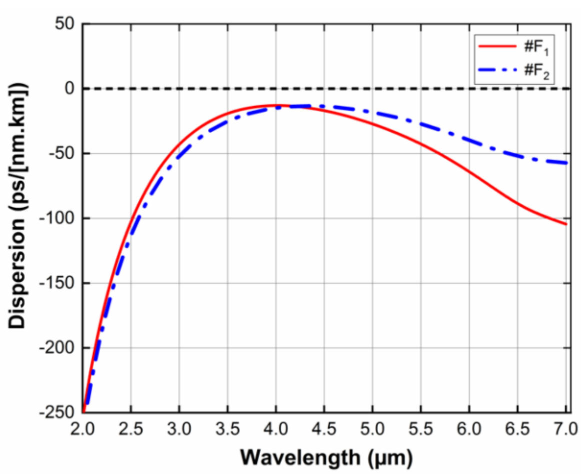

Figure 7. The chromatic dispersion of the proposed PCFs

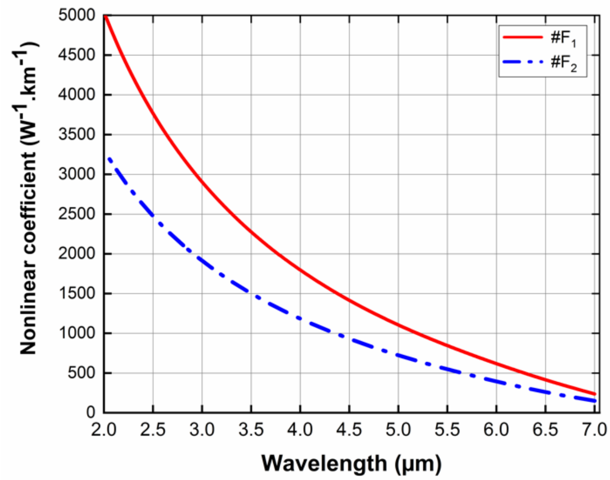

Figure 8. The nonlinear coefficient of the proposed PCFs

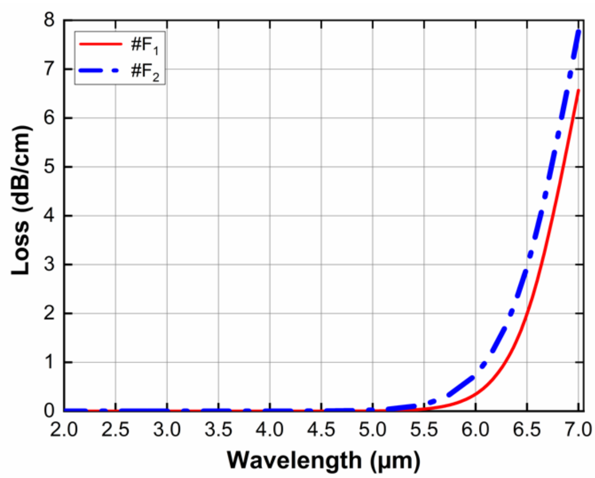

Figure 9. The confinement loss of the proposed PCFs

Figures 6–9 confirm the nonlinear characteristics of the proposed PCFs, where the red curves show the nonlinear properties of the #F_1 fiber and the blue curves show the properties of the #F_2 fiber. The real part of the effective refraction index is always higher for the #F_2 fiber than the #F_1 fiber at all survey wavelengths, which is the reason for the flatter dispersion and closer approach to zero of the #F_2 fiber. In the wavelength region from 2 to 4.3 μm, the #F_2 fiber has lower dispersion, but this value exceeds the dispersion of the #F_1 fiber in the rest of the wavelength regime. Moreover, the larger core has reduced the nonlinear coefficient and increased the confinement loss of the #F_2 fiber. It should be noted that it is difficult to optimize all nonlinear properties of PCFs simultaneously. Depending on the application purpose, we have set control of how the structure is designed as a priority. In this case, both selected PCFs are suitable for SC generation because of their dispersion dominance. In this paper, we chose the pumped wavelength as 4.5 μm, closest to the wavelength of the maximum dispersion. The values of the nonlinear characteristics at this wavelength are given in Table 7.

Table 7. Nonlinear characteristics of the proposed PCFs at 4.5 µm wavelength

#	$Re[n_{\text{eff}}]$	D (ps.nm^{-1}.km^{-1})	γ (W^{-1}.km^{-1})	L_c (dB/cm)
#F_1	2.07	-16.88	1414.709	3.075E-04
#F_2	2.089	-13.63	931.194	2.98E-03

4. CONCLUSIONS

With the new design featuring an inhomogeneous structure of air hole diameters, we simulated 24 PCF structures and analyzed their nonlinear characteristics in detail. The outstanding point of this study is that the PCFs exhibit wide variation in dispersion, high nonlinear coefficients, and small confinement loss. Based on the numerical simulation results, two proposed PCFs have acceptable all-normal, flat, near-zero dispersion properties, and small confinement loss, which are excellent conditions to orient the SC generation with a broad spectrum. Our proposed fibers, because of their high nonlinearity, low loss, and optimal dispersion, open a promising future for all-fiber SC generation sources as an alternative to glass-core fibers.

ACKNOWLEDGMENTS

This research is funded by the Vietnam Ministry of Education and Training under grant number B2021-DHH-08.

REFERENCES

Bishwas, M. S., Ahmad, R., Kabir, M. R., Hossen, I., Ul Islam, A. S. M. T., & Faruqe, O. (2021). Mid-infrared supercontinuum generation in AS_2Se_3 glass based C_2H_5OH filled square photonic crystal fiber. *2021 International Conference on Information and Communication Technology for Sustainable Development* (ICICT4SD) (pp. 245-248).

Biswas, B., Ahmed, K., Paul, B. K., Khalek, Md. A., & Uddin, M. S. (2019). Numerical evaluation of the performance of different materials in nonlinear optical applications. *Results in Physics*, *13*, 102184. https://doi.org/10.1016/j.rinp.2019.102184

Buczyński, R. (2004). Photonic crystal fibers. *Acta Physica Polonica Series A, 106*, 141-168. https://doi.org/10.12693/APhysPolA.106.141

Chauhan, P., Kumar, A., & Kalra, Y. (2020). Numerical exploration of coherent supercontinuum generation in multicomponent $GeSe_2$-As_2Se_3-PbSe chalcogenide based photonic crystal fiber. *Optical Fiber Technology*, *54*, 102100. https://doi.org/10.1016/j.yofte.2019.102100

Cherif, R., Salem, A. B., Zghal, M., Besnard, P., Chartier, T., Brilland, L., & Troles, J. (2010). Highly nonlinear As_2Se_3-based chalcogenide photonic crystal fiber for midinfrared supercontinuum generation. *Optical Engineering*, *49*(9), 095002-6. https://doi.org/10.1117/1.3488042

Eid, M. M. A., Habib, Md. A., Anower, Md. S., & Rashed, A. N. Z. (2021). Highly sensitive nonlinear photonic crystal fiber based sensor for chemical sensing applications. *Microsystem Technologies*, *27*(3), 1007-1014. https://doi.org/10.1007/s00542-020-05019-w

Gao, W., Zhang, X., Jiang, W., Zhang, Z., Gao, P., Chen, L., Wang, P., Zhang, W., Wang, R., Liao, M., Suzuki, T., Ohishi, Y., & Zhou, Y. (2020). Characteristics of vector beams in mid-infrared waveband in an As_2Se_3 photonic crystal fiber with small hollow core. *Optical Fiber Technology*, *55*(9), 102152. https://doi.org/10.1016/j.yofte.2020.102152

Hasan, M. M., Barid, M., Hossain, Md. S., Sen, S., & Azad, M. M. (2021). Large effective area with high power fraction in the core region and extremely low effective material loss-based photonic crystal fiber (PCF) in the terahertz (THz) wave pulse for different types of communication sectors. *Journal of Optics*, *50*(14), 681-688. https://doi.org/10.1007/s12596-021-00740-9

Hui, Z., Yang, M., Zhang, Y., & Zhang, M. (2018). Mid-infrared high birefringence As_2Se_3-based PCF with large nonlinearity and distinctive dispersion by using asymmetric elliptical air hole cladding. *Modern Physics Letters B*, *32*(03), 1850023. https://doi.org/10.1142/S0217984918500239

Kabir, Md. A., Ahmed, K., Hassan, Md. M., Hossain, Md. M., & Pau, B. K. (2020). Design a photonic crystal fiber of guiding terahertz orbital angular momentum beams in optical communication. *Optics Communications*, *475*, 126192. https://doi.org/10.1016/j.optcom.2020.126192

Karim, M. R., Ahmad, H., Ghosh, S., & Rahman, B. M. A. (2018). Mid-infrared supercontinuum generation using As_2Se_3 photonic crystal fiber and the impact of higher-order dispersion parameters on its supercontinuum bandwidth. *Optical Fiber Technology*, *45*, 255-266. https://doi.org/10.1016/j.yofte.2018.07.024

Kaur, V., & Singh, S. (2019). Design of titanium nitride coated PCF-SPR sensor for liquid sensing applications. *Optical Fiber Technology*, *48*, 159-164. https://doi.org/10.1016/j.yofte.2018.12.015

Knight, J. C. (2003). Photonic crystal fibres. *Nature*, *424*(6950), 847-851. https://doi.org/10.1038/nature01940

Lanh, C. V., Hoang, V. T., Long, V. C., Borzycki, K., Khoa, D. X., Quoc, V. T., Trippenbach, M., Buczyński, R., & Pniewski, J. (2019). Optimization of optical properties of photonic crystal fibers infiltrated with chloroform for supercontinuum generation. *Laser Physics*, *29*(7), 075107. https://doi.org/10.1088/1555-6611/ab2115

Lanh, C. V., Hoang, V. T., Long, V. C., Borzycki, K., Khoa, D. X., Quoc, V. T., Trippenbach, M., Buczyński, R., & Pniewski, J. (2020). Supercontinuum generation in photonic crystal fibers infiltrated with nitrobenzene. *Laser Physics*, *30*(3), 035105. https://doi.org/10.1088/1555-6611/ab6f09

Li, F., He, M., Zhang, X., Chang, M., Wu, Z., Liu, Z., & Chen, H. (2018). Elliptical As_2Se_3 filled core ultra-high-nonlinearity and polarization-maintaining photonic crystal fiber with double hexagonal lattice cladding. *Optical Materials, 79,* 137-146. https://doi.org/10.1016/j.optmat.2018.03.025

Markin, A. V., Markina, N. E., & Goryacheva, I. Yu. (2017). Raman spectroscopy based analysis inside photonic-crystal fibers. *TrAC Trends in Analytical Chemistry*, *88*, 185-197. https://doi.org/10.1016/j.trac.2017.01.003

Mohammadzadehasl, N., & Noori, M. (2019). Design of low-loss and near-zero ultraflattened dispersion PCF for broadband optical communication. *Photonics and Nanostructures - Fundamentals and Applications*, *35*(7), 100703. https://doi.org/10.1016/j.photonics.2019.100703

Park, K., Na, J., Kim, J, & Jeong, Y. (2020). Numerical study on supercontinuum generation in an active highly nonlinear photonic crystal fiber with anomalous dispersion. *IEEE Journal of Quantum Electronics, 56*(2), 6800109.

Paul, B. K., Ahmed, K., Dhasarathan, V., Al-Zahrani, F. A., Aktar, Mst. N., Uddin, M. S., & Aly, A. H. (2020). Investigation of gas sensor based on differential optical absorption spectroscopy using photonic crystal fiber. *Alexandria Engineering Journal*, *59*(6), 5045-5052. https://doi.org/10.1016/j.aej.2020.09.030

Paul, B. K., Rajesh, E., Asaduzzaman, S., Islam, Md. S., Ahmed, K., Amiri, I. S., & Zakaria, R. (2018). Design and analysis of slotted core photonic crystal fiber for gas sensing application. *Results in Physics*, *11*, 643-650. https://doi.org/10.1016/j.rinp.2018.10.004

Podder, E., Hossain, Md. B., Jibon, R. H., Bulbul, A. A.-M., & Mondal, H. S. (2019). Chemical sensing through photonic crystal fiber: Sulfuric acid detection. *Frontiers of Optoelectronics*, *12*, 372-381. https://doi.org/10.1007/s12200-019-0903-8

Qi, X., Chen, S., Li, Z., Liu, T., Ou, Y., Wang, N., & Hou, J. (2018). High-power visible-enhanced all-fiber supercontinuum generation in a seven-core photonic crystal fiber pumped at 1016 nm. *Optics Letters*, *43*(5), 1019-1022. https://doi.org/10.1364/OL.43.001019

Saini, T. S., Kumar, A., & Sinha, R. K. (2015). Broadband mid-IR supercontinuum generation in As_2Se_3 based chalcogenide photonic crystal fiber: A new design and analysis. *Optics Communications*, *347*, 13-19. https://doi.org/10.1016/j.optcom.2015.02.049

Saitoh, K., Koshiba, M., Hasegawa, T., & Sasaoka, E. (2003). Chromatic dispersion control in photonic crystal fibers: Application to ultra-flattened dispersion. *Optics Express, 11*(8), 843-852. https://doi.org/10.1364/OE.11.000843

Ung, B., & Skorobogatiy, M. (2010). Chalcogenide microporous fibers for linear and nonlinear applications in the mid-infrared. *Optics Express*, *18*(8), 8647-8659. https://doi.org/10.1364/OE.18.008647

Wang, X. Y., Li, S. G., Liu, S., Yin, G. B., & Li, J. S. (2012). Generation of a mid-infrared broadband polarized supercontinuum in As_2Se_3 photonic crystal fibers. *Chinese Physics B*, *21*(5), 054220. https://doi.org/10.1088/1674-1056/21/5/054220

Zhao, T., Lian, Z., Benson, T., Wang X., Zhang, W., & Lou, S. (2017). Highly-nonlinear polarization-maintaining As_2Se_3-based photonic quasi-crystal fiber for supercontinuum generation. *Optical Materials*, *73*, 343-349. https://doi.org/10.1016/j.optmat.2017.07.010